HHS Public Access

Author manuscript

J Mol Med (Berl). Author manuscript; available in PMC 2021 March 01.

Published in final edited form as:

J Mol Med (Berl). 2020 March ; 98(3): 425–435. doi:10.1007/s00109-020-01883-1.

Spatial localization of endothelial cells in heterotypic spheroids influences NOTCH signaling

Charlotte E. Vorwald[a], **Shreeya Joshee**[a], **J. Kent Leach**[a,b]

[a]Department of Biomedical Engineering, University of California, Davis, Davis, CA, 95616

[b]Department of Orthopaedic Surgery, UC Davis Health, Sacramento, CA 95817

Abstract

Cell-based therapeutic approaches are an exciting strategy to replenish compromised endothelial cell (EC) populations that contribute to impaired vasculogenesis. Co-cultures of ECs and mesenchymal stromal cells (MSCs) can enhance neovascularization over ECs alone, but the efficacy of cells is limited by rapid cell death upon implantation. Co-culture spheroids exhibit improved survival compared to monodisperse cells, yet little is known about the influence of spatial regulation of ECs within co-culture spheroids. We hypothesized that EC sprouting from co-culture spheroids is a function of EC spatial localization. We formed co-culture spheroids containing ECs and MSCs in two formats: ECs uniformly distributed throughout the spheroid (*i.e.*, mixed) or seeded on the perimeter of the MSC core (*i.e.*, shell). Qualitative observations suggested increased vasculogenesis for mixed co-culture spheroids compared to shell conformations as early as Day 3, yet quantitative metrics did not reveal significant differences in network formation between these 3D structures. Notch3 expression demonstrated significant increases in cell-cell communication in mixed conformations compared to shell counterparts. Furthermore, knockdown of Notch3 in MSCs abrogated the vasculogenic potential of mixed spheroids, supporting its role in promoting EC-MSC contacts. This study highlights the direct impact of EC-MSC contacts on sprouting and provides insight to improve the quality of network formation.

Keywords

vascularization; spheroids; endothelial cell; mesenchymal stromal cell; NOTCH

INTRODUCTION

There is an urgent need to restore vascularization for treating peripheral vascular disease or compromised wounds [1]. Local delivery of potent angiogenic growth factors are under investigation to guide new blood vessel formation but are limited by rapid degradation, high

Address for correspondence: J. Kent Leach, Ph.D., Department of Biomedical Engineering, University of California, Davis, 451 Health Sciences Drive, Davis, CA 95616, jkleach@ucdavis.edu.

CONFLICT OF INTEREST

The authors have no conflict of interest.

requisite dosages, and potential side effects [2, 3]. Current methods are inconsistent and stress the need for autologous cell-based approaches that provide the necessary building blocks to form the vasculature. Tissue engineering seeks to address this challenge by delivering patients' own cells within instructive biomaterial constructs to accelerate the native, regenerative capacity of wounds. Strategies to recapitulate environments that allow for cells' innate capacity to remodel and form vasculature are under investigation. It is essential to understand the process of such self-assembled vasculature to support a host of tissue regeneration applications that require nutrient supply [4].

Endothelial cells (ECs) are broadly studied for use in neovascularization strategies, as they directly form blood vessels during vasculogenesis [5]. The structural integrity and persistence of nascent vessels can be improved by the addition or recruitment of supportive mural cells [6]. Among candidate mural cells, mesenchymal stromal cells (MSCs) reside in the perivascular niche and exhibit key pericytic functions, promoting blood vessel stabilization and maturation [7, 8] Furthermore, MSCs can promote capillary maturation *in vivo* better than other stromal cell populations [9]. For example, the transplantation of MSCs with ECs resulted in decreased vessel leakiness compared to ECs alone or EC-fibroblast co-cultures. Thus, the synergy of ECs with MSCs provides an exciting opportunity to enhance the efficacy of cell-based approaches to neovascularization.

While ECs and MSCs demonstrate the functional capacity to form vasculature, the retention of function and survival upon implantation remains a challenge. We and others have demonstrated the promise of spheroid formation as a tool to improve survival [10, 11] and preserve cell-cell contacts necessary for angiogenic processes [12–16]. Furthermore, the benefits of spheroid delivery have been demonstrated by utilizing EC-MSC aggregates to retain network capacity [17] and construct pre-vascularization [18]. Although important, these studies assess the potential of co-culture spheroids from homogeneously mixed suspensions. According to the Differential Adhesion Hypothesis, cells in aggregates possess an innate capacity to sort over time [19], driven by cadherin expression to maximize mutual binding and minimize surface tension.

While this sorting phenomena can be observed in long-term spheroid culture [20, 21], the effect of sorting and spatial organization on therapeutic capacity is unknown. We hypothesized that endothelial cell sprouting from co-culture spheroids is a function of initial endothelial cell spatial localization. Here, we describe a method to control localization of endothelial cells within EC-MSC co-culture spheroids and compare the vasculogenic potential to standard mixed co-culture formation. We observed the effect of spatial organization on sprout morphology and mesh formation, which led to our exploration of possible mechanisms behind these phenomena. This work reveals strategies to enhance communication between key cell populations to ultimately define strategies that improve network formation.

MATERIALS AND METHODS

Cell culture

Human cord blood-derived endothelial colony forming cells were provided by Dr. Eduardo Silva (UC Davis) and expanded in EGM-2 supplemented with gentamycin (50 μg/mL) and amphotericin B (50 ng/mL) (PromoCell, Heidelberg, Germany) under standard conditions (37°C, 5% CO_2, 21% O_2) until use at passage 5–8 [22]. Human bone marrow derived MSCs (Lonza, Walkersville, MD) from a single donor (22-year-old male) were expanded without further characterization in growth medium (GM) consisting of minimum essential alpha medium (α-MEM; Invitrogen, Carlsbad, CA) supplemented with 10% fetal bovine serum (FBS; Atlanta Biologicals, Flowery Branch, GA) and 1% penicillin/streptomycin (Gemini Bio-Products, Sacramento, CA). MSCs were cultured under standard conditions until use at passage 5. Media changes were performed every 2–3 days. For each experiment, aliquots were derived from the same batch of serum to ensure consistency.

Spheroid formation

ECs and MSCs were formed into spheroids using a high throughput forced gravitational method [23]. ECs and MSCs were seeded onto agarose molds with 29 pre-defined wells at a final concentration of 4.35×10^5 cells/mL in a 24-well plate and centrifuged at 163×*g* for 8 min to form “mixed” spheroids containing 10,000 MSCs and 5,000 ECs (15,000 cells/spheroid). For 10,000 and 5,000 cells/spheroid controls, cell suspension volumes were adjusted accordingly before centrifugation. Aggregates were incubated at 37°C for 48 h to allow spheroid formation. To create EC shell spheroids, MSC spheroids (10,000 cells/spheroid) were formed as described above. After 48 h of formation, media was removed from each well, ECs were gently pipetted directly on aggregates at 1.45×10^5 cells/mL (5,000 cells/spheroid), and spheroids were centrifuged at 163×*g* for 8 min. Aggregates were incubated at 37°C for 24 h to allow EC adhesion and resultant “shell” spheroids (Fig. 1).

Spheroid encapsulation in fibrin gel

After formation of EC-MSC spheroids (Fig. 1), we assessed EC and MSC localization *via* confocal microscopy. Spheroids were encapsulated in fibrin gels on angiogenesis μ-slides (ibidi GmbH, Planegg, Germany). Fibrinogen (10 mg/mL) (Millipore Sigma, Darmstadt, Germany) was dissolved in 3:1 EGM-2:α-MEM. For each group, media was removed from one spheroid well and spheroids were released from wells with 1 mL of fibrinogen solution. 9 μL of suspension containing one spheroid was added to each well with 1 μL of 50 U/mL thrombin (Millipore Sigma) to yield a final concentration of 2.5 U/mL thrombin and 10 mg/mL fibrinogen. Gels were allowed to form at 37°C for 30 min. 50 μL of 3:1 media was added to each well and media changes were performed every 2 days.

Evaluation of sprouting *via* confocal microscopy

Before spheroid formation, ECs were stained with CellTrace™ Oregon Green® 488 (carboxy-DFFDA SE) and MSCs were stained with CellTrace™ Far Red Cell Proliferation Kit (both from Invitrogen). Confocal microscopy was performed using the Leica TCS SP8 (Leica, Wetzlar, Germany). Images were acquired as 2D slices and processed and analyzed

in ImageJ (NIH, Bethesda, MD). For analysis of images, confocal images were converted to 500 × 500 pixel size, converted to binary, and quantified using the Angiogenesis Analyzer plugin. Segments were defined as lines connected to other components on both ends. Branches were defined as lines that are connected to a segment on one end and free on the other. Meshes were defined as closed loops of segments. Total length was defined as the total of segments, branches and isolated elements in the analyzed area [24]. Values are reported by cell population channel acquired for each spheroid group.

PCR

Total RNA was collected and isolated in Trizol (Thermo Fisher Scientific, Waltham, MA), and 800 ng of total RNA was reverse transcribed with the QuantiTect Reverse Transcription Kit (Qiagen). qPCR was performed using TaqMan1 Universal PCR Master Mix (Applied Biosystems). Primers and probes consisted of *NOTCH1* (Hs01062014_m1), *NOTCH2* (Hs01050702_m1), *NOTCH3* (Hs01128537_m1), *NOTCH4* (Hs00965889_m1), *JAG1* (Hs01070032_m1), *JAG2* (Hs00171432_m1), and *DLL4* (Hs00184092_m1). Amplification conditions were 50°C for 2 min, 95°C for 10 min, followed by 40 cycles at 95°C for 15 s and 60°C for 1 min. Quantitative PCR results were normalized to *RPL13* (Hs00204173_m1) transcript level to yield ΔCt. Values are represented as $2^{-\Delta Ct}$.

Notch 3 detection by immunohistochemistry and immunofluorescence

Fibrin gels were fixed in 10% buffered formalin for 4 h at room temperature and washed in PBS. Samples were dehydrated, processed, and paraffin-embedded overnight. Each gel was sectioned at 5 μm thickness using a Leica RM2235 Manual Rotary Microtome for subsequent staining. For CD31 and smooth-muscle actin (SMA) immunofluorescence, slides were dehydrated and processed for antigen retrieval using chondroitinase ABC (Millipore Sigma). Primary antibodies against CD31 (1:20; ab28364, Abcam, Cambridge, MA) and SMA (1:50; ab7817, Abcam) were incubated overnight at 4°C. Biotin-conjugated anti-rabbit (1:100; ab6720, Abcam) and anti-mouse (1:200; B7151, Sigma) secondary antibodies were added and incubated at room temperature for 1 h. ExtrAvidin-FITC and -Cy3 (1:100; Sigma) were added to CD31 and SMA samples, respectively, and incubated for 1 h at room temperature. DAPI (2 μg/mL; Thermo Fisher) was added and incubated at room temperature for 10 min and mounted with VECTASHIELD Antifade Mounting Medium (Vector Laboratories, Burlingame, CA). Images were acquired *via* fluorescence microscopy with the Nikon Eclipse TE2000U. EC only and MSC only spheroids served as controls. For Notch3 expression experiments, processing and staining was performed as described above. Heat-mediated antigen retrieval was performed. Staining consisted of Notch3 (5 μg/mL; ab23426; Abcam), along with biotin-conjugated anti-rabbit (1:100; ab6720, Abcam) with ExtrAvidin-FITC (1:100; Sigma). Human breast carcinoma tissue served as the positive control for Notch3 expression.

Notch3 knockdown in MSCs *via* siRNA and subsequent spheroid formation

siRNA encoding for *GAPDH* (cat. #4390849), *NOTCH3* (cat. #4392420), or a scrambled negative control (cat. #4390846; all from Thermo Fisher) was condensed with branched 25 kDa PEI (Millipore Sigma) at an N/P ratio = 12 [25]. MSCs (5×10^4 cells/well in 6-well plates) were transfected in monolayer culture with 2 μg of PEI-siRNA complexes suspended

in 500 μL of Opti-MEM Reduced Serum Media (Life Technologies). After 4 h of incubation, media was refreshed to remove PEI-siRNA complexes, and MSCs were cultured for 3 days until characterized or used to make spheroids. Mixed and shell spheroids containing 5,000 MSCs and 2,500 ECs (7,500 cells/spheroid) were formed and used as described above. Mixed and shell spheroids containing MSCs without transfection served as positive controls.

Notch3 knockdown was confirmed in MSCs by Western blotting. MSCs were lysed and homogenized with a 30G needle in RIPA buffer (Thermo Fisher), and all lysates were cleared by centrifugation. Protein concentration was determined with a Pierce BCA Protein Assay Kit (Thermo Fisher). HeLa cell lysate (BD Biosciences, San Jose, CA) was used as a negative control for Notch3, while untreated MSC spheroids were used as positive controls for GAPDH, Beta-actin, and Notch3. Equal amounts of protein were loaded onto a 10% Nu-PAGE Tris-Acetate Gel (Invitrogen) and resolved by gel electrophoresis. Proteins were transferred using the iBlot system (Invitrogen). Membranes were blocked with blocking buffer (2.5% nonfat dry milk in TBS, Tween-20, and ultrapure H_2O). Primary Notch3 rat monoclonal antibody (mAB) (1:1000, #3446; Cell Signaling Technology, Danvers, MA), primary Beta-actin rabbit mAB (1:1000, #4970; Cell Signaling) and GAPDH rabbit mAB (1:1000, #5174; Cell Signaling) were added in blocking buffer as recommended by the manufacturer. Membranes were washed with 10× TBS, Tween-20, and ultrapure H_2O. Anti-rat IgG HRP-linked (1:1000, #7077; Cell Signaling) and Anti-rabbit IgG HRP-linked antibody (1:1000, #7074; Cell Signaling Technology) was added in blocking buffer. Membranes were washed, and detection was performed using the ChemiDoc MP Imaging System (BioRad, Hercules, CA).

Statistical analysis

Data are presented as means ± standard deviation from at least three biological replicates and one biological donor from each cell population. Statistical significance was assessed by either ordinary one-way ANOVA or two-Way ANOVA with Tukey's multiple comparisons test, and p-values <0.05 were considered statistically significant. Statistical analysis was performed using GraphPad Prism® 8 analysis software (GraphPad Software, La Jolla, CA). Different letters denote statistical significance between groups.

RESULTS

EC spatial localization can be manipulated in EC-MSC spheroids

We observed key differences in EC localization between "mixed" and "shell" formation methods at Day 0 (Fig. 2A). ECs were interspersed in mixed co-culture spheroids, while ECs in shell counterparts were localized on the periphery of the spheroids. To confirm the spatial distribution of ECs and MSCs, we performed immunohistochemistry for CD31 and SMA, respectively (Fig. 2B and Supplementary Fig. 1). In agreement with confocal microscopy, CD31 and SMA localization revealed differences in EC and MSC localization between mixed and shell configurations.

EC-MSC sprouting patterns are dependent upon EC localization

To understand the effect of EC localization in co-culture spheroids on vasculogenic potential, we suspended EC-MSC spheroids in fibrin gel and assessed sprouting over 7 days *via* confocal microscopy (Fig. 3A–B). Clear differences in morphology were observed on Day 3, with ECs in shell spheroids exhibiting farther migration from the spheroid periphery and less surface area in contact with MSCs. In mixed spheroids, ECs formed intermittent, elongated structures and remained clustered among MSCs around the spheroid perimeter. Quantification of EC and MSC populations are presented separately in each group and timepoint to delineate the EC sprouting and MSC supporting roles during the angiogenic process. These metrics revealed no significant differences between mixed and shell conformations for either EC or MSC populations on Day 3 or Day 7. On Day 7, we observed differences between homotypic MSC spheroids and co-culture spheroids. Among several metrics exhibiting significant differences between MSC and mixed spheroids, the most notable parameters included number of segments (68.1 ± 60.6 vs. 124.4 ± 34.0; p=0.001) (Fig. 3C), number of branches (51.3 ± 35.3 vs. 72.9 ±18.9; p=0.01) (Fig. 3D), total segment length (2501.6 ± 2337.7 μm vs. 5533.5 ± 1679.5 μm; p<0.0001) (Fig. 3F), and branch length (2265.3 ± 1397.6 μm vs. 3523.1 ± 836.7 μm; p=0.0008) (Fig. 3G). Across all parameters, shell and mixed spheroids demonstrated increased sprouting compared to monodisperse counterparts (Supplementary Fig. 2). ECs exhibited increased number of meshes (Fig. 3E) and similar trends in mean mesh size (Fig. 3H) in the presence of MSCs.

EC-MSC co-culture spheroids influence NOTCH signaling

After observing differences in EC and MSC migration and sprout morphology, we hypothesized that EC localization in EC-MSC spheroids influences NOTCH signaling, a critical pathway for embryogenesis and development [26]. To test this, we collected EC-MSC spheroids on Day 0 for gene expression of key Notch signaling receptors (*NOTCH1, −2, −3, and −4*) and Jagged1 and DLL4 ligands (*JAG1* and *DLL4*, respectively) (Fig. 4). *NOTCH3* expression was significantly lower in shell spheroids compared to mixed spheroids (p=0.02) and statistically similar to homotypic MSC control spheroids. *NOTCH3* was not detected in homotypic EC spheroids, while *NOTCH4* and *DLL4* expression was not detected in homotypic MSC spheroids. To understand differences in the Notch pathway upstream, we investigated NOTCH3 protein expression *via* immunofluorescence (Fig. 5). Despite differences in gene expression, NOTCH3 expression was downregulated in both EC and shell spheroids compared to homotypic MSC spheroids, with mixed spheroids exhibiting intermediate expression among all groups.

Notch3 knockdown in MSCs abrogates vasculogenic potential of EC-MSC spheroids

To elucidate the role of Notch3 on vasculogenic potential, we used siRNA to knock down NOTCH3 in MSCs (Supplementary Fig. 3). Notch3 expression was low in siRNA-treated monolayer groups, and GAPDH siRNA-treated MSC controls had significant reduction in protein expression. Furthermore, beta-actin expression was similar across all groups, confirming that the lack of Notch3 and GAPDH signal was due to effective treatment, not off-target siRNA action. We formed EC-MSC spheroids in both mixed and shell conformations, and interrogated sprouting potential in fibrin gel over 7 days *via* confocal

microscopy (Fig. 6). At Day 3, MSCs in mixed control spheroids exhibited significantly increased sprouting potential compared to siRNA-treated MSC mixed spheroid counterparts (Fig. 6A). These qualitative observations were supported by significant quantitative reductions in the number of segments (50.5 ± 11.0 vs. 19.0 ± 9.9; $p<0.0001$), branches (36.3 ± 10.7 vs. 21.0 ± 5.7; $p=0.03$), and meshes (4.5 ± 2.5 vs. 0.8 ± 1.3; $p=0.004$), segment length (2237.8 ± 242.0 vs. 667.6 ± 436.5 μm; $p<0.0001$), and branch length (1964.0 ± 767.2 vs. 1013.8 ± 329.7 μm; $p=0.02$) (Fig. 6B–F). On Day 3, untreated MSCs in mixed and shell groups exhibited differences in number of segments (50.5 ± 11.0 and 19.3 ± 5.2; $p<0.0001$), number of meshes (4.50 ± 2.5 and 0.8 ± 0.5; $p=0.006$), and segment length (2237.8 ± 242.0 and 829.3 ± 139.8 μm; $p<0.0001$). Mesh size was similar between both cell types and timepoints (Fig. 6G). At Day 7, we only observed differences in branch length (1825.0 ± 473.8 vs. 1077.6 ± 370.0 μm; $p=0.02$) between naïve and NOTCH3-knockdown MSCs in mixed spheroids. We did not observe quantitative differences between EC populations.

DISCUSSION

Cell-based therapies provide building blocks to rapidly restore function and improve the local environment in a damaged wound site. Spheroid formation has been extensively studied as a platform to increase cell viability and function, as they retain ECM components that drive key cell-cell communication pathways [11, 27]. In aggregate form, heterotypic co-cultures including ECs and MSCs exhibit an innate capacity to undergo cell sorting, triggering multiple signal transduction cues for vascular network formation [16]. Here, we investigate whether network formation can be influenced by regulating initial spatial positioning of ECs, thereby allowing these processes to naturally progress or artificially controlling the spatial organization. Our data reveal differences in network formation among EC and MSC populations between heterotypic spheroids and homotypic counterparts. These data demonstrate the role of EC localization within co-culture spheroids on vasculogenic potential, confirming the participation of NOTCH signaling between ECs and MSCs during spheroid formation. The results of this study are particularly exciting because they demonstrate the effect of EC spatial localization in EC-MSC spheroids and highlight the importance of EC-MSC self-sorting to drive formation of consistent vascular structures.

We observed distinct EC localization patterns in shell and mixed groups during spheroid assembly. Moreover, we confirmed that mixed co-culture strategies are effective in supporting EC-MSC communication for vasculogenic potential. We studied the effect of spatially localizing ECs within EC-MSC co-culture spheroids on sprouting potential. We chose a 1:2 ratio of ECs to MSCs to create a thick, distinct shell layer. The delivery of monodisperse stromal cell populations with ECs at this ratio and cell concentration yields stable vascular structures *in vitro* and *in vivo* [28, 29], confirming the ability of stromal cells to promote vascular retention. We successfully created EC shells on MSC spheroids using our centrifugation method [23]. While others have observed EC localization in the periphery of heterotypic organoids over time after cell sorting [30], many have investigated the effect on vasculogenic potential post self-assembly. EC localization is dynamic, and cell-cell interactions during cell sorting of spheroids are essential to drive fate and function. By forming an EC shell around MSC spheroids, we could decouple EC localization and EC-MSC interactions during the self-assembly process, effectively accelerating the sorting of

ECs to the surface that occurs over time in co-culture spheroids. Shell formation accelerates the innate assembly of these populations but disconnects them from downstream signaling needed for robust tube formation. We previously observed robust sprouting from homotypic EC spheroids in fibrin gels that surpassed network formation by monodisperse ECs over 24 hours [12]. However, proangiogenic growth factors such as VEGF and FGF present within complete culture media were insufficient to retain network formation by EC spheroids by Day 7. This suggests the key contribution of MSCs in network stabilization, as well as differences in network formation with mixed and shell conformations.

Fibrin has been extensively studied as an extracellular matrix to monitor cell migration due to its role as a provisional matrix in native wound healing and during remodeling [31]. The use of a 3D matrix to assess the vasculogenic potential of spheroids offers a host of benefits compared to frequently used 2D Matrigel platforms [17] and collagen beads [32, 33]. We used fibrin gels with 10 mg/mL fibrinogen for increasing EC-stromal vasculogenic potential as previously reported [28], although lower concentrations can also yield effective results [34]. Key cell-cell contacts are lost in monolayer and bead surfaces alike, failing to fully recapitulate cell-cell signaling pathways to initiate sprout determination and potentially resulting in misleading findings. We compared spheroids to monodisperse co-culture populations to demonstrate the differences in network formation with each format (Supplementary Fig. 2). We observed differences in increased sprout formation of heterotypic cultures when studied as spheroids versus monodispersed cells in fibrin gels. At Day 3 of spheroid culture, ECs in shell groups migrated farther from spheroid surfaces but formed more disorganized structures compared to mixed counterparts. Conversely, mixed spheroids exhibited more dense localization towards the center of the spheroid and distinct sprouts. At Day 7, we observed the presence of tubule structures in mixed groups. ECs in shell groups at this timepoint resulted in variable structures farther from spheroid surfaces exhibiting migration. We did not detect statistical differences in vasculogenic parameters such as segment, branch, and mesh numbers between shell and mixed groups. However, these data clearly demonstrate the increased potential of co-culture spheroids compared to homotypic counterparts, while stressing the importance of stromal-endothelial cell interactions. The quantification of complex, 3D structures with 2D slices does not fully capture this angiogenic phenomenon, and others have demonstrated similar challenges when using similar methods [35]. Since we quantified 3D networks using a 2D image, some qualities of these constructs are not captured, such as lumen formation and vessel thickness, representing a limitation of this study.

The dynamic rearrangement of cells within aggregates follows the Differential Adhesion Hypothesis, with cells sorting to maximize their adhesion strength and minimize free energy for development [19, 36, 37]. Spheroids represent an ideal platform to observe these phenomena while investigating their vasculogenic potential. However, this hypothesis is primarily supported by the role of cadherins, transmembrane proteins supporting cell-cell contact and implicated in vascular permeability [38]. More recently, NOTCH signaling has been identified as a key modulator of cell fate and function of endothelial cells [39]. Human MSCs and ECs can express these receptors, and others have shown that NOTCH signaling can coordinate tip versus stalk cell fate within a developing sprout [40]. DLL4 and Jagged1 are key ligands that modulate this process, activating tip and stalk cell status, respectively

[41]. In these studies, we detected differences in *NOTCH3*, *DLL4*, and *JAG1* expression between mixed and shell groups. We observed the greatest NOTCH3 expression in both homotypic MSC spheroids and mixed spheroids, with diminished signal in shell spheroids. Despite some observed differences in *NOTCH1*, *−2*, and *−4* expression between mixed and shell groups, differences in *NOTCH3* were most apparent and significant, motivating our selection of Notch3 for further interrogation. Evaluation of the role of other Notch proteins on sprouting in spheroids merits future investigation. Others have recognized NOTCH3 expression in SMA+ pericytes [42, 43] and demonstrated its role in platelet-derived growth factor (PDGF-BB) maintenance of pericyte survival [44]. PDGF-BB is a potent angiogenic growth factor secreted by activated platelets and endothelial tip cells to attract surrounding mural cells, initiating a cascade of events leading to stalk cell quiescence and basement membrane deposition [45]. Differences in *DLL4* were detected between homotypic EC and MSC spheroids, with intermediate expression in both mixed and shell groups. This may suggest higher DLL4 and Jagged1 signaling to NOTCH-expressing cells in co-culture, with possibly more controlled activation in co-culture spheroids. We speculate that NOTCH3 expression is a function of MSC-MSC contact and may be more tightly regulated upon EC presence. As the importance of NOTCH3 endothelial-mural cell activation has been reported [46] and silencing can promote tumor angiogenesis [47], tuning the regulation of this receptor may be necessary. Through siRNA knockdown of NOTCH3, these data provide further evidence that NOTCH3 has an important role in vasculogenesis from co-culture spheroids. Further investigation of NOTCH protein activation and degradation is warranted to understand the role of this signaling pathway on regulating EC responsiveness to such growth factors to ultimately unlock their vasculogenic potential.

These findings provide key insight into EC-MSC contact regulation for neovascularization. Our data reveal the importance of direct EC-MSC crosstalk in spheroids for consistent vasculogenic potential. The improved qualitative morphology of networks observed in confocal images using mixed co-culture spheroids confirms that regulation of EC localization to the periphery suppresses the necessary endogenous physical cues to instruct vessel formation. This was supported by observed differences in NOTCH3 expression, a well-established cell-cell receptor known to drive pericytic functions during angiogenesis. Overall, these studies highlight an essential signal transduction pathway for EC-MSC network formation while providing a platform to deploy cell-based therapies for vasculogenesis.

Supplementary Material

Refer to Web version on PubMed Central for supplementary material.

ACKNOWLEDGEMENTS

Research reported in this publication was supported by National Institute of Dental and Craniofacial Research of the National Institutes of Health under award number R01 DE025475 (JKL). CEV was supported by the NHLBI Training Program in Basic and Translational Cardiovascular Science (T32 HL086350). The content is solely the responsibility of the authors and does not necessarily represent the official views of the National Institutes of Health. We acknowledge Eduardo Silva for providing cord blood-derived endothelial cells and Alena Casella for early contributions to this work.

REFERENCES

1. Shen YI, Cho H, Papa AE, Burke JA, Chan XY, Duh EJ, Gerecht S (2016) Engineered human vascularized constructs accelerate diabetic wound healing. Biomaterials 102: 107–119. DOI 10.1016/j.biomaterials.2016.06.009 [PubMed: 27328431]
2. Matkar PN, Ariyagunarajah R, Leong-Poi H, Singh KK (2017) Friends turned foes: angiogenic growth factors beyond angiogenesis. Biomolecules 7 DOI 10.3390/biom7040074
3. Lu LX, Deegan A, Musa F, Xu T, Yang Y (2018) The effects of biomimetically conjugated VEGF on osteogenesis and angiogenesis of MSCs (human and rat) and HUVECs co-culture models. Colloids Surf B Biointerfaces 167: 550–559. DOI 10.1016/j.colsurfb.2018.04.060 [PubMed: 29730577]
4. Juhas M, Engelmayr GC Jr., Fontanella AN, Palmer GM, Bursac N (2014) Biomimetic engineered muscle with capacity for vascular integration and functional maturation in vivo. Proc Natl Acad Sci U S A 111: 5508–5513. DOI 10.1073/pnas.1402723111 [PubMed: 24706792]
5. Chang WG, Niklason LE (2017) A short discourse on vascular tissue engineering. NPJ Regen Med 2 DOI 10.1038/s41536-017-0011-6
6. Kaigler D, Krebsbach PH, Polverini PJ, Mooney DJ (2003) Role of vascular endothelial growth factor in bone marrow stromal cell modulation of endothelial cells. Tissue Eng 9: 95–103. DOI Doi 10.1089/107632703762687573 [PubMed: 12625958]
7. Ghajar CM, Blevins KS, Hughes CC, George SC, Putnam AJ (2006) Mesenchymal stem cells enhance angiogenesis in mechanically viable prevascularized tissues via early matrix metalloproteinase upregulation. Tissue Eng 12: 2875–2888. DOI 10.1089/ten.2006.12.2875 [PubMed: 17518656]
8. Ghajar CM, Kachgal S, Kniazeva E, Mori H, Costes SV, George SC, Putnam AJ (2010) Mesenchymal cells stimulate capillary morphogenesis via distinct proteolytic mechanisms. Exp Cell Res 316: 813–825. DOI 10.1016/j.yexcr.2010.01.013 [PubMed: 20067788]
9. Grainger SJ, Carrion B, Ceccarelli J, Putnam AJ (2013) Stromal cell identity influences the in vivo functionality of engineered capillary networks formed by co-delivery of endothelial cells and stromal cells. Tissue Eng Part A 19: 1209–1222. DOI 10.1089/ten.TEA.2012.0281 [PubMed: 23216113]
10. Murphy KC, Whitehead J, Falahee PC, Zhou D, Simon SI, Leach JK (2017) Multifactorial experimental design to optimize the anti-inflammatory and proangiogenic potential of mesenchymal stem cell spheroids. Stem Cells 35: 1493–1504. DOI 10.1002/stem.2606 [PubMed: 28276602]
11. Murphy KC, Fang SY, Leach JK (2014) Human mesenchymal stem cell spheroids in fibrin hydrogels exhibit improved cell survival and potential for bone healing. Cell Tissue Res 357: 91–99. DOI 10.1007/s00441-014-1830-z [PubMed: 24781147]
12. Vorwald CE, Murphy KC, Leach JK (2018) Restoring vasculogenic potential of endothelial cells from diabetic patients through spheroid formation. Cell Mol Bioeng 11: 267–278. DOI 10.1007/s12195-018-0531-1 [PubMed: 30416603]
13. Ho SS, Murphy KC, Binder BY, Vissers CB, Leach JK (2016) Increased survival and function of mesenchymal stem cell spheroids entrapped in instructive alginate hydrogels. Stem Cells Transl Med 5: 773–781. DOI 10.5966/sctm.2015-0211 [PubMed: 27057004]
14. Roux BM, Akar B, Zhou W, Stojkova K, Barrera B, Brankov J, Brey EM (2018) Preformed vascular networks survive and enhance vascularization in critical sized cranial defects. Tissue Eng Part A 24: 1603–1615. DOI 10.1089/ten.TEA.2017.0493 [PubMed: 30019616]
15. Bhang SH, Lee S, Lee TJ, La WG, Yang HS, Cho SW, Kim BS (2012) Three-dimensional cell grafting enhances the angiogenic efficacy of human umbilical vein endothelial cells. Tissue Eng Part A 18: 310–319. DOI 10.1089/ten.TEA.2011.0193 [PubMed: 21902465]
16. Song LQ, Yuan XG, Jones Z, Griffin K, Zhou Y, Ma T, Li Y (2019) Assembly of human stem cell-derived cortical spheroids and vascular spheroids to model 3-D brain-like tissues. Sci Rep 9 DOI 10.1038/s41598-019-42439-9
17. Chen DY, Wei HJ, Lin KJ, Huang CC, Wang CC, Wu CT, Chao KT, Chen KJ, Chang Y, Sung HW (2013) Three-dimensional cell aggregates composed of HUVECs and cbMSCs for therapeutic

neovascularization in a mouse model of hindlimb ischemia. Biomaterials 34: 19952004. DOI 10.1016/j.biomaterials.2012.11.045

18. Bauman E, Feijao T, Carvalho DTO, Granja PL, Barrias CC (2018) Xeno-free prevascularized spheroids for therapeutic applications. Sci Rep 8 DOI 10.1038/s41598-017-18431-6
19. Foty RA, Steinberg MS (2005) The differential adhesion hypothesis: a direct evaluation. Dev Biol 278: 255–263. DOI 10.1016/j.ydbio.2004.11.012 [PubMed: 15649477]
20. Marshall J, Barnes A, Genever P (2018) Analysis of the intrinsic self-organising properties of mesenchymal stromal cells in three-dimensional co-culture models with endothelial cells. Bioengineering (Basel) 5 DOI 10.3390/bioengineering5040092
21. Clevers H (2016) Modeling development and disease with organoids. Cell 165: 1586–1597. DOI 10.1016/j.cell.2016.05.082 [PubMed: 27315476]
22. Williams PA, Stilhano RS, To VP, Tran L, Wong K, Silva EA (2015) Hypoxia augments outgrowth endothelial cell (OEC) sprouting and directed migration in response to sphingosine-1-phosphate (S1P). PLoS One 10(4):e0123437. DOI 10.1371/journal.pone.0123437.
23. Vorwald CE, Ho SS, Whitehead J, Leach JK (2018) High-throughput formation of mesenchymal stem cell spheroids and entrapment in alginate hydrogels. Methods Mol Biol 1758: 139–149. DOI 10.1007/978-1-4939-7741-3_11 [PubMed: 29679328]
24. Carpentier G, Cascone I (2012) Angiogenesis Analyzer for ImageJ. ImageJ User and Developer Conference 2012.
25. Gonzalez-Fernandez T, Sathy BN, Hobbs C, Cunniffe GM, McCarthy HO, Dunne NJ, Nicolosi V, O'Brien FJ, Kelly DJ (2017) Mesenchymal stem cell fate following non-viral gene transfection strongly depends on the choice of delivery vector. Acta Biomater 55: 226–238. DOI 10.1016/j.actbio.2017.03.044 [PubMed: 28363788]
26. Andersson ER, Sandberg R, Lendahl U (2011) Notch signaling: simplicity in design, versatility in function. Development 138: 3593–3612. DOI 10.1242/dev.063610 [PubMed: 21828089]
27. Baraniak PR, McDevitt TC (2012) Scaffold-free culture of mesenchymal stem cell spheroids in suspension preserves multilineage potential. Cell Tissue Res 347: 701–711. DOI 10.1007/s00441-011-1215-5 [PubMed: 21833761]
28. Moya ML, Hsu YH, Lee AP, Hughes CC, George SC (2013) In vitro perfused human capillary networks. Tissue Eng Part C Methods 19: 730–737. DOI 10.1089/ten.TEC.2012.0430 [PubMed: 23320912]
29. Chen X, Aledia AS, Popson SA, Him L, Hughes CCW, George SC (2010) Rapid anastomosis of endothelial progenitor cell-derived vessels with host vasculature is promoted by a high density of cotransplanted fibroblasts. Tissue Eng Part A 16: 585–594. DOI 10.1089/ten.TEA.2009.0491 [PubMed: 19737050]
30. Hsu SH, Ho TT, Huang NC, Yao CL, Peng LH, Dai NT (2014) Substrate-dependent modulation of 3D spheroid morphology self-assembled in mesenchymal stem cell-endothelial progenitor cell coculture. Biomaterials 35: 7295–7307. DOI 10.1016/j.biomaterials.2014.05.033 [PubMed: 24909102]
31. Weisel JW, Litvinov RI (2017) Fibrin formation, structure and properties. Subcell Biochem 82: 405–456. DOI 10.1007/978-3-319-49674-0_13 [PubMed: 28101869]
32. Nakatsu MN, Davis J, Hughes CC (2007) Optimized fibrin gel bead assay for the study of angiogenesis. J Vis Exp: 186 DOI 10.3791/186
33. Nowak-Sliwinska P, Alitalo K, Allen E, Anisimov A, Aplin AC, Auerbach R, Augustin HG, Bates DO, van Beijnum JR, Bender RHF, et al. (2018) Consensus guidelines for the use and interpretation of angiogenesis assays. Angiogenesis 21: 425–532. DOI 10.1007/s10456-018-9613-x [PubMed: 29766399]
34. Bezenah JR, Kong YP, Putnam AJ (2018) Evaluating the potential of endothelial cells derived from human induced pluripotent stem cells to form microvascular networks in 3D cultures. Sci Rep 8: 2671 DOI 10.1038/s41598-018-20966-1 [PubMed: 29422650]
35. Rindone AN, Kachniarz B, Achebe CC, Riddle RC, O'Sullivan AN, Dorafshar AH, Grayson WL (2019) Heparin-conjugated decellularized bone particles promote enhanced osteogenic signaling of PDGF-BB to adipose-derived stem cells in tissue engineered bone grafts. Adv Healthc Mat 8 DOI 10.1002/adhm.201801565

36. Steinberg MS, Takeichi M (1994) Experimental specification of cell sorting, tissue spreading, and specific spatial patterning by quantitative differences in cadherin expression. Proc Natl Acad Sci U S A 91: 206–209. DOI 10.1073/pnas.91.1.206 [PubMed: 8278366]
37. Steinberg MS, Gilbert SF (2004) Townes and Holtfreter (1955): directed movements and selective adhesion of embryonic amphibian cells. J Exp Zool A Comp Exp Biol 301: 701–706. DOI 10.1002/jez.a.114 [PubMed: 15559931]
38. Amack JD, Manning ML (2012) Knowing the boundaries: extending the differential adhesion hypothesis in embryonic cell sorting. Science 338: 212–215. DOI 10.1126/science.1223953 [PubMed: 23066072]
39. Mack JJ, Iruela-Arispe ML (2018) NOTCH regulation of the endothelial cell phenotype. Current Opin Hematol 25: 212–218. DOI 10.1097/Moh.0000000000000425
40. Hasan SS, Tsaryk R, Lange M, Wisniewski L, Moore JC, Lawson ND, Wojciechowska K, Schnittler H, Siekmann AF (2017) Endothelial Notch signalling limits angiogenesis via control of artery formation. Nat Cell Biol 19: 928–940. DOI 10.1038/ncb3574 [PubMed: 28714969]
41. Pitulescu ME, Schmidt I, Giaimo BD, Antoine T, Berkenfeld F, Ferrante F, Park H, Ehling M, Biljes D, Rocha SF, et al. (2017) Dll4 and Notch signalling couples sprouting angiogenesis and artery formation. Nat Cell Biol 19: 915–927. DOI 10.1038/ncb3555 [PubMed: 28714968]
42. Winkler EA, Sagare AP, Zlokovic BV (2014) The pericyte: a forgotten cell type with important implications for Alzheimer's disease? Brain Pathol 24: 371–386. DOI 10.1111/bpa.12152 [PubMed: 24946075]
43. Wimmer RA, Leopoldi A, Aichinger M, Wick N, Hantusch B, Novatchkova M, Taubenschmid J, Hammerle M, Esk C, Bagley JA, et al. (2019) Human blood vessel organoids as a model of diabetic vasculopathy. Nature 565: 505–510. DOI 10.1038/s41586-018-0858-8 [PubMed: 30651639]
44. Wang Y, Pan L, Moens CB, Appel B (2014) Notch3 establishes brain vascular integrity by regulating pericyte number. Development 141: 307–317. DOI 10.1242/dev.096107 [PubMed: 24306108]
45. Peters EB (2018) Endothelial progenitor cells for the vascularization of engineered tissues. Tissue Eng Part B Rev 24: 1–24. DOI 10.1089/ten.TEB.2017.0127 [PubMed: 28548628]
46. Liu H, Kennard S, Lilly B (2009) NOTCH3 expression is induced in mural cells through an autoregulatory loop that requires endothelial-expressed JAGGED1. Circ Res 104: 466–U497. DOI 10.1161/Circresaha.108.184846 [PubMed: 19150886]
47. Lin S, Negulescu A, Bulusu S, Gibert B, Delcros JG, Ducarouge B, Rama N, Gadot N, Treilleux I, Saintigny P, et al. (2017) Non-canonical NOTCH3 signalling limits tumour angiogenesis. Nat Commun 8: 16074. DOI 10.1038/ncomms16074

Key Messages:

- Endothelial cell (EC) localization can be controlled in co-culture EC-MSC spheroids
- Mixed spheroids exhibit consistent networks compared to shell counterparts
- Differences in *NOTCH3* was observed between mixed and shell spheroids
- *NOTCH3* may be a necessary target for improved vasculogenic potential

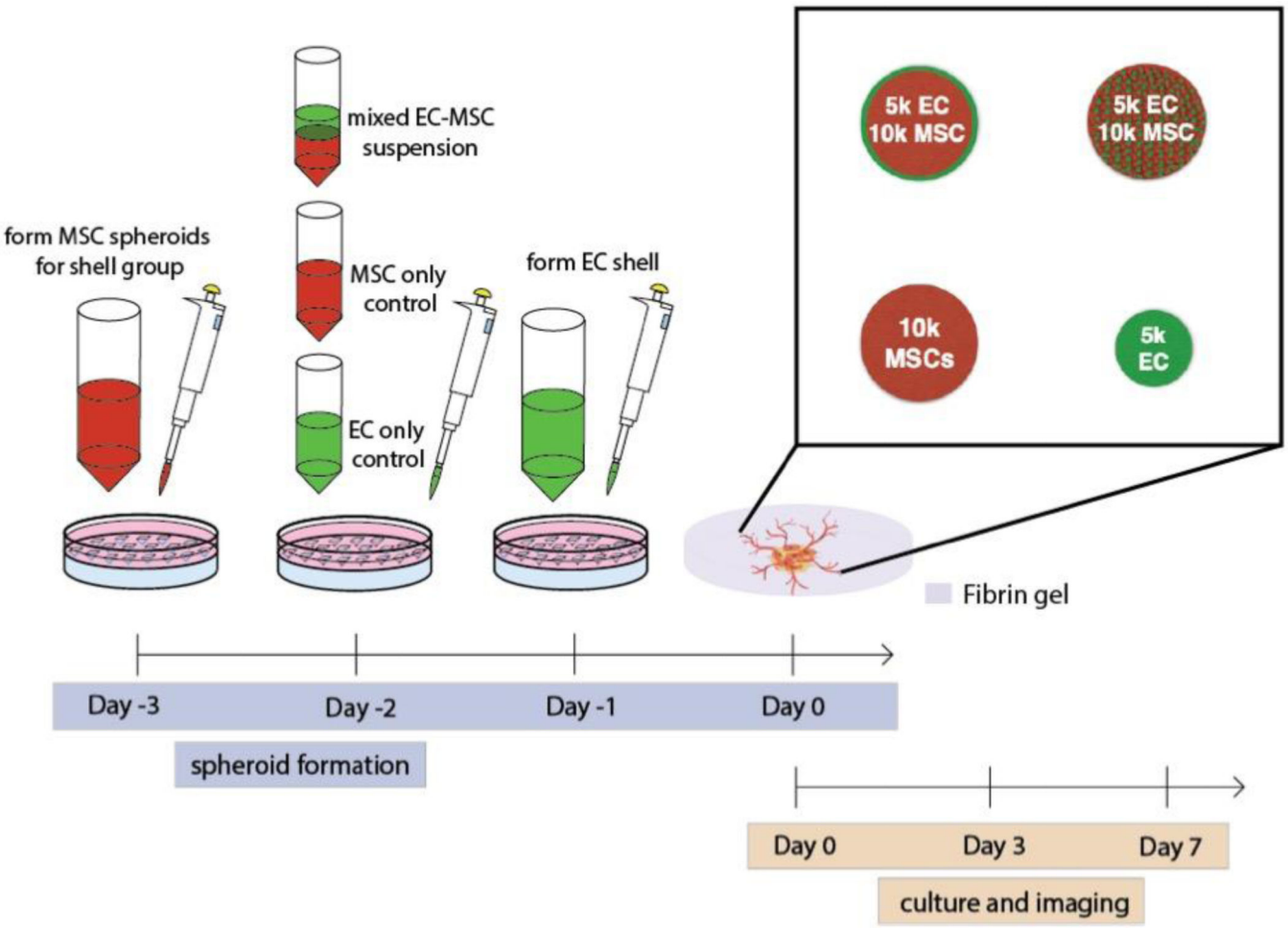

Figure 1.
Experimental outline of EC-MSC spheroid shell formation and analysis.

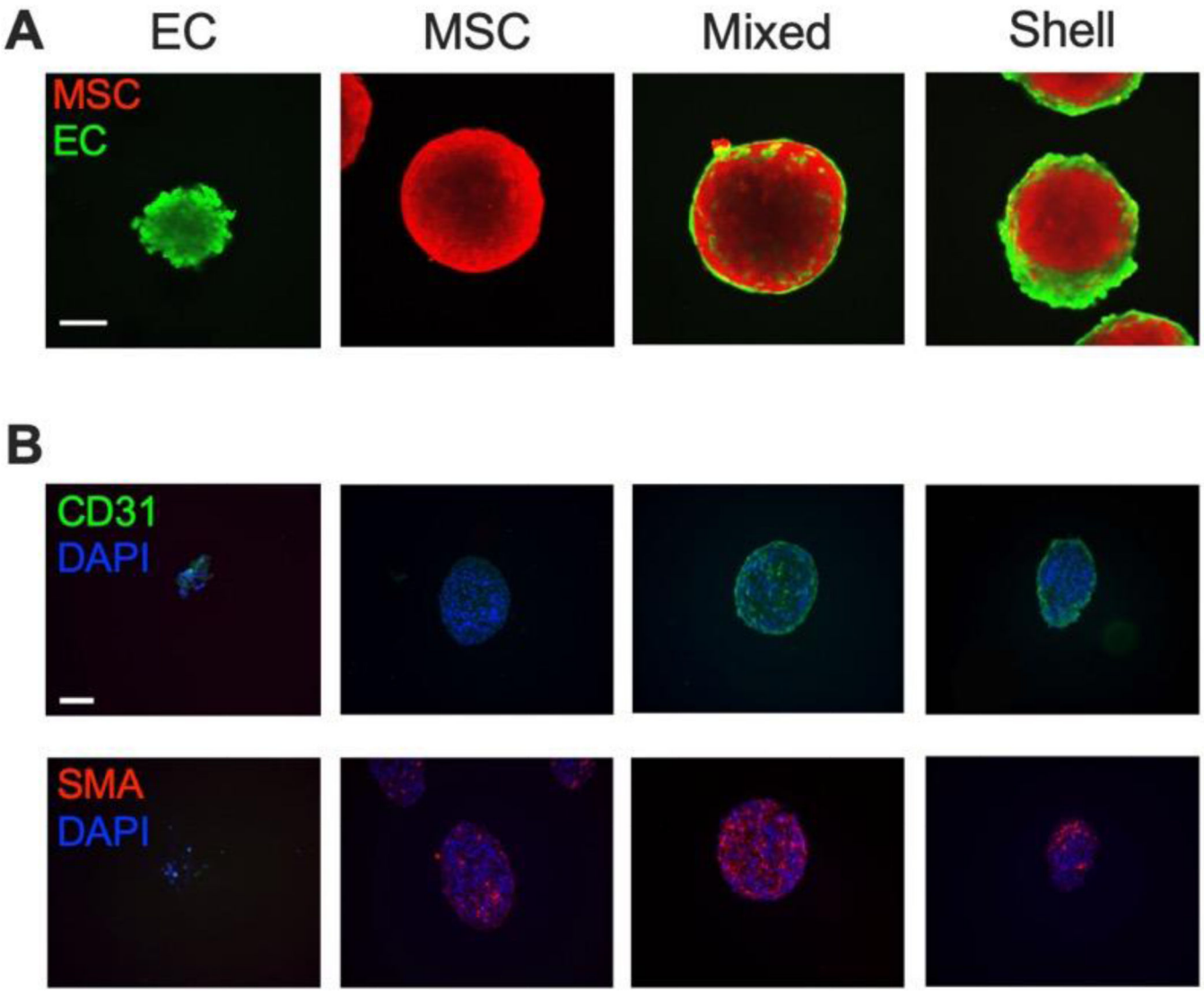

Figure 2. Spatial localization of ECs can be controlled in EC-MSC spheroids.

(A) Confocal images of EC-MSC spheroids in suspension on Day 0. ECs are green; MSCs are red. Scale bar = 100 μm. **(B)** CD31 and SMA staining of EC-MSC spheroids on Day 0. CD31 is green; SMA is red; DAPI is blue. Scale bar = 100 μm.

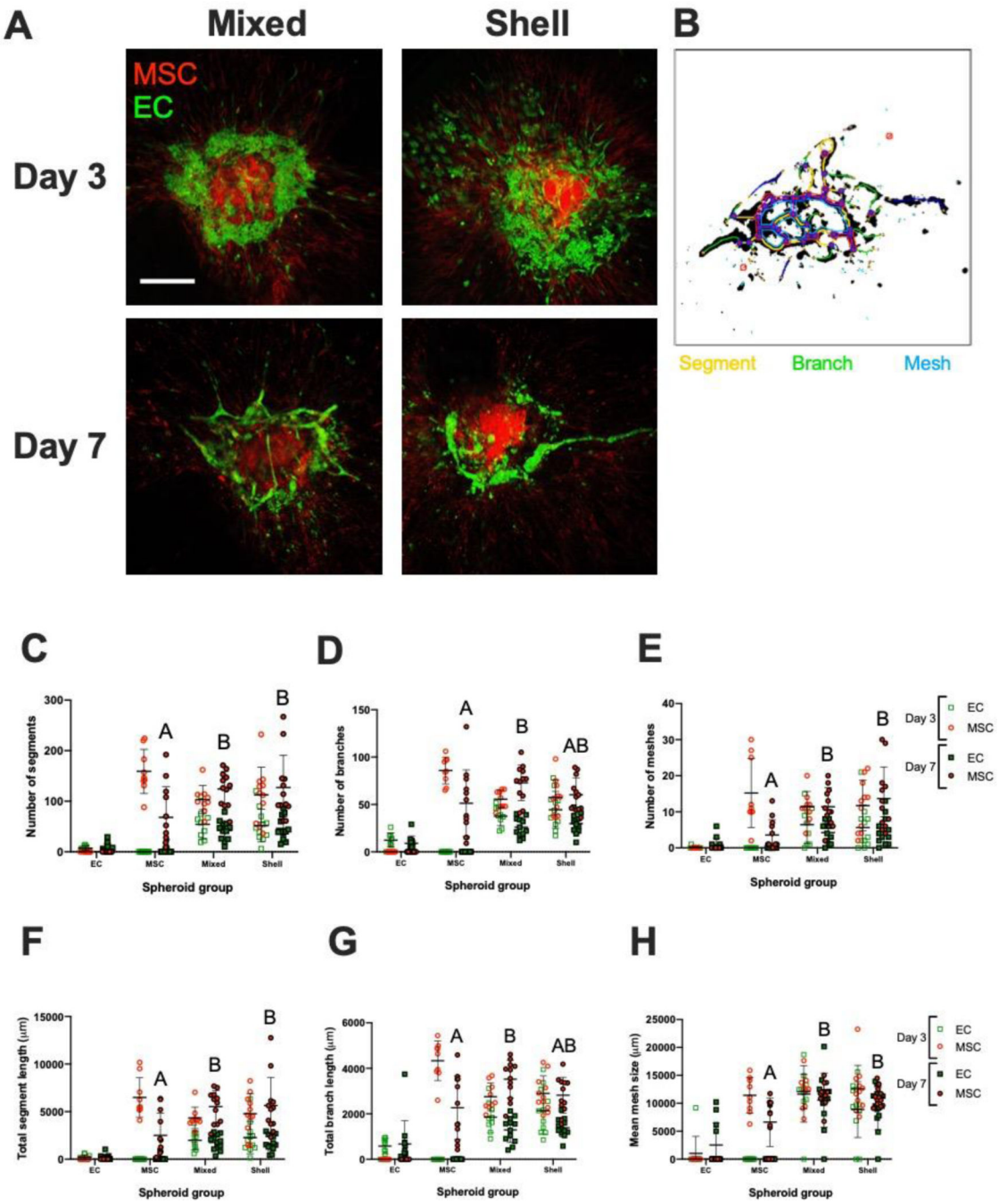

Figure 3. EC-MSC sprouting patterns in fibrin gel on Day 3 and Day 7.

(A) Confocal images of EC-MSC mixed and shell spheroids in fibrin gel on Days 3 and 7. ECs are green; MSCs are red. Scale bar = 250 μm. **(B)** Representative overlay of spheroid with quantification metrics to visualize segments (yellow), branches (green), and meshes (blue). **(C)** Number of segments **(D)** number of branches, and **(E)** number of meshes in field of view on Day 3 and Day 7 separated by population channel for each spheroid group. **(F)** Total segment length **(G)** total branch length **(H)** and mean mesh size in field of view on Day 3 and Day 7 separated by population channel for each spheroid group. Chart values

represent mean ± standard deviation (n=9–12); open markers denote Day 3 while filled markers refer to Day 7. Different letters denote statistical significance of MSC populations between groups.

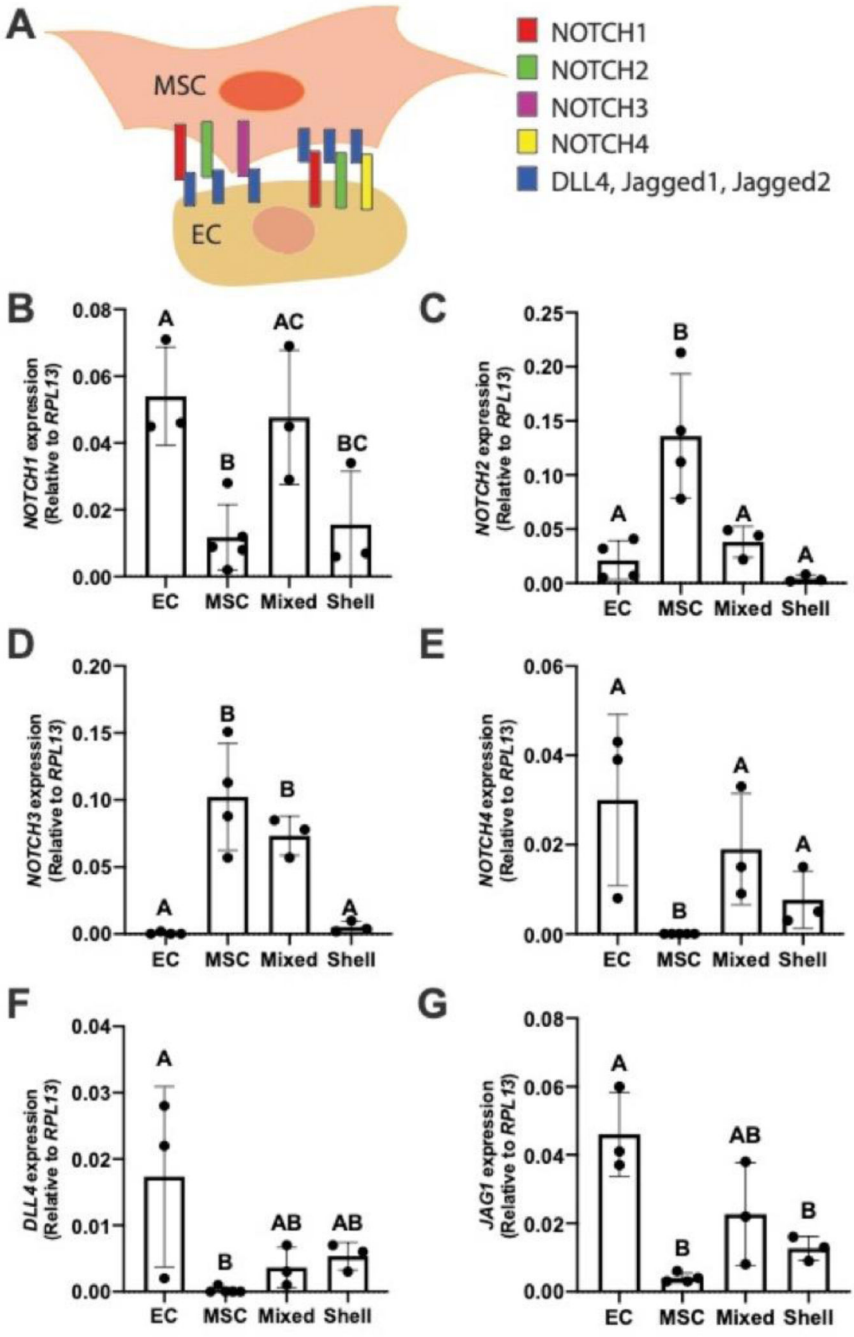

Figure 4. EC localization influences NOTCH signaling in EC-MSC co-culture spheroids.

(A) Illustration of NOTCH expression of MSC and ECs with respective ligands. **(B)** *NOTCH1* **(C)** *NOTCH2* **(D)** *NOTCH3* **(E)** *NOTCH4* **(F)** *DLL4* **(E)** and *JAG1* expression. Chart values represent mean ± standard deviation (n=3–5). Different letters denote statistical significance between groups.

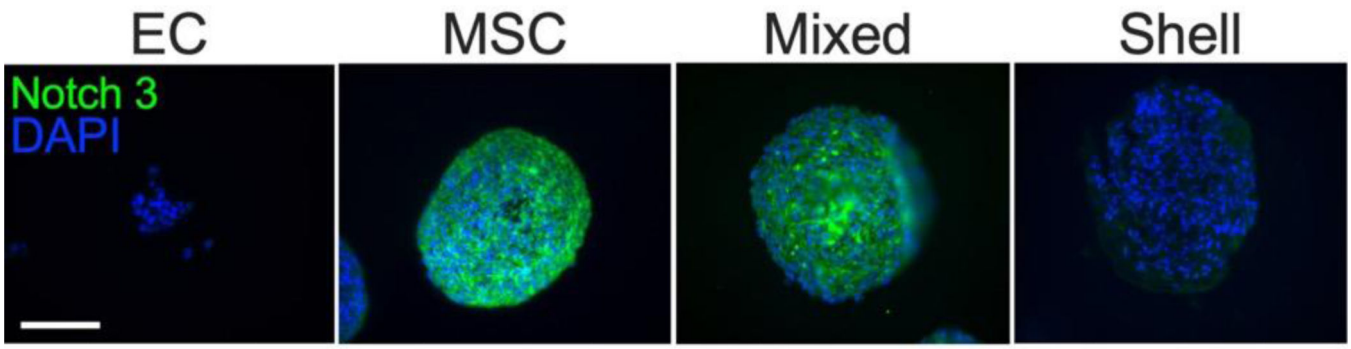

Figure 5. NOTCH3 patterns in shell and mixed EC-MSC spheroids upon formation.
Notch3 protein is green; DAPI is blue. Scale bar = 100 μm.

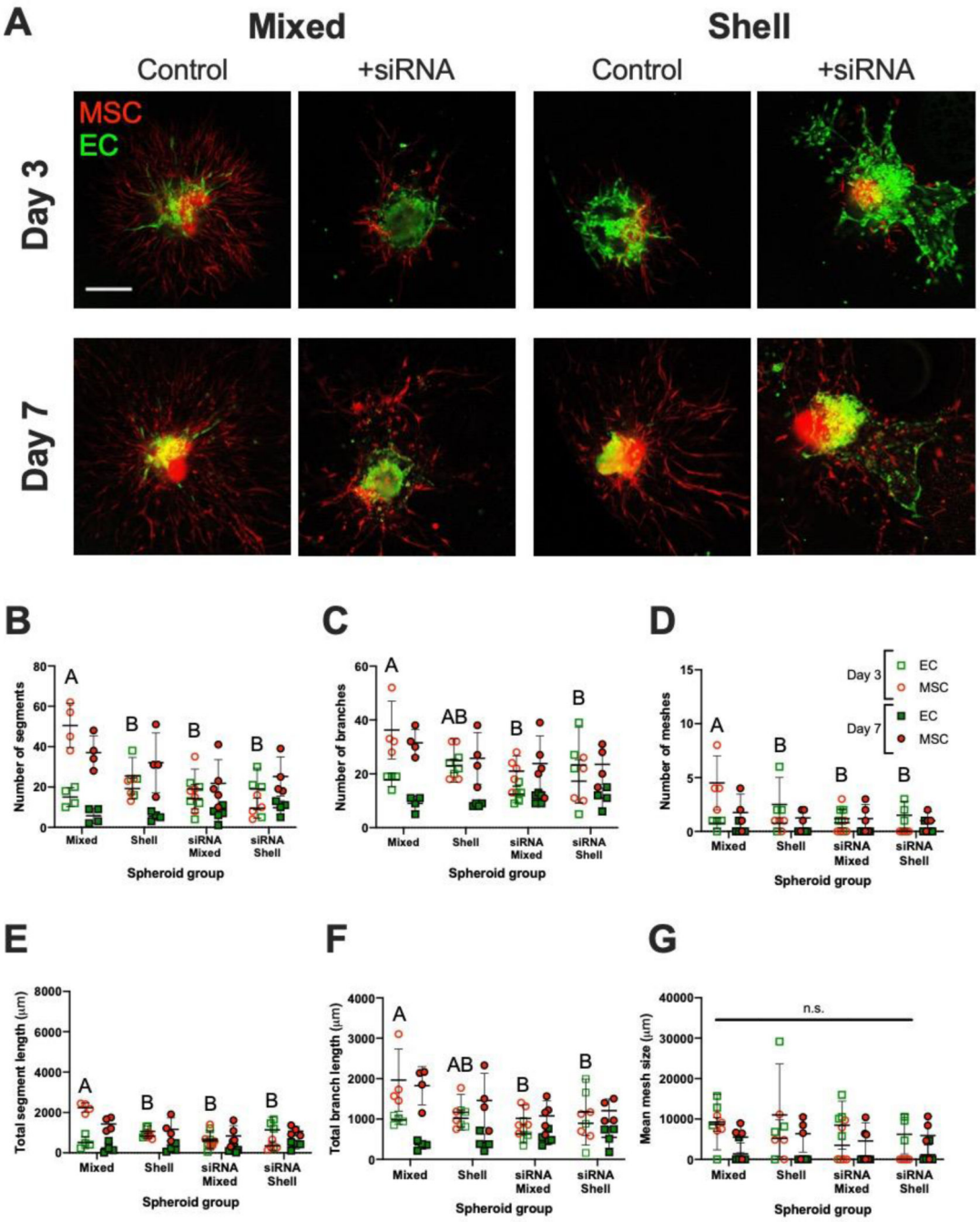

Figure 6. Notch3 knockdown *via* siRNA abrogates MSC sprouting in mixed EC-MSC spheroids.

(A) Confocal images of EC-MSC mixed and shell spheroids in fibrin gel on Day 3 and Day 7 with or without MSC siRNA treatment; ECs are green, MSCs are red. Scale bar = 100 μm. Number of **(B)** segments, **(C)** branches, and **(D)** meshes in field of view on Day 3 and Day 7 separated by population channel for each spheroid group. **(E)** Total segment length, **(F)** total branch length, **(G)** and mean mesh size in field of view on Day 3 and Day 7 separated by population channel for each spheroid group. Chart values represent mean ± standard deviation (n=4–5); open markers denote Day 3 while filled markers refer to Day 7. Different

letters denote statistical significance between MSC groups on Day 3; no statistical differences were observed at Day 7.